Path Planning Approach for a Quadrotor Unmanned Aerial Vehicle

César A. Cárdenas R.[1(✉)], V. Landero[2], Ramón E. R. González[3],
Paola Ariza-Colpas[4], Emiro De-la-Hoz-Franco[4],
and Carlos Andrés Collazos-Morales[1(✉)]

[1] Vicerrectoria de Investigaciones, Universidad Manuela Beltrán, Bogotá, Colombia
{cesar.cardenas,carlos.collazos}@docentes.umb.edu.co
[2] Universidad Politécnica de Apodoca, Apodaca, Nuevo León, Mexico
[3] Departamento de Física, Universidade Federal Rural de Pernambuco, Recife,
Pernambuco, Brazil
[4] Departamento de Ciencias de la Computación y Electrónica,
Universidad de la Costa, Barranquilla, Colombia

Abstract. A path planning method for an unmanned aerial system type quadrotor is proposed in this work. It is based on Dubins curves. Therefore, different points (initial and ending) are set for generation of several paths. Additionally, to validate the proposed model a computational resource is applied. Also, some flight dynamics limits and orientation angles computations are considered to be able to determine a simplified Dubins model. Dubins paths are commonly divided into low, medium and high altitude gains. It will depend on the altitude established for the start and end points and other configurations.

Keywords: Dubins · VTOL · Flight dynamics · Path planning

1 Introduction

Motion planning involves path as well as trajectory planning. Path planning is a very important matter regarding unmanned autonomous vehicles. It can be defined as a search of a feasible path starting at any initial point to a final one in which a collision-free environment can be obtained. Hence, kinematic limitations of the system can be met. It is significant to point that there is a difference between path and trajectory planning. The first one considers the path geometry. The other one is more related to how a path evolves over time. Thus, in this research a path planning with 2D Dubins curves is developed and proposed. Moreover, other 3D paths are also generated similar to the ones studied in [15,16]. Dubins paths designed for aerial vehicles are indeed more difficult due to the altitude changes. It looks like short paths will be able reduce consumption of fuel, travel time, energy and even life cycle of the platform. An unmanned aircraft flying at a steady altitude might save fuel. To determine an appropriate path planning approach, a vehicle and an aeronautics or aerospace

reference frame have to be defined. Also, a 2D path planning option could help to a path with an unchanging altitude. So, path planning is a very remarkable issue to ensure that an unmanned aircraft can travel considerable distance missions completely. [13, 17–19].

2   Dubins Curves

As it is presented in [8], to be able to find a short path between two points, a mixture of lines and circular segments is needed. As stated earlier, Dubins paths can be classified as low, medium, or high altitude gains. Therefore, both altitude changes and steady altitude are looked into. There are three possibilities for a body to travel. These are straight lines, left and right curves. The resulting paths can be either CCC or CSC. C describes a circular arc in which the radius is ρ or R_{min}. S shows a straight line. This is method known as the Dubins path. Hence, some of path configurations that can be got from a Dubins are: $D = LSL, LSR, RSR, RSL, LRL, RLR$. The arcs should be a left (L) and right (R) turn illustration and (S) is a straight line. The first point is for Dubins path generation is to establish what type of path will be employed. [9, 11]. Similary, other path planning options can be found in [1, 4, 5].

3   Dubins Aircraft Model

An airplane should be considered to move with a continuous velocity v and a steady altitude h. Thus, g is neglected since an aerial vehicle will be taken. So, the 2D system is as follows:

Dubins' car model: **Dubins' aerial vehicle model:**

$$\begin{bmatrix} \dot{x} \\ \dot{y} \\ \dot{\psi} \end{bmatrix} = \begin{bmatrix} cos\ \psi \\ sin\ \psi \\ u \end{bmatrix} \qquad \begin{bmatrix} \dot{x} \\ \dot{y} \\ \dot{\psi} \end{bmatrix} = \begin{bmatrix} v\ cos\ \psi \\ v\ sin\ \psi \\ \omega \end{bmatrix} \qquad (1)$$

where ω is the turning rate of the aircraft, v is the velocity, x and y are the inertial position and ψ is the heading angle.

3.1   Dubins Paths

For Dubins paths generation that can be feasible, it is necessary to consider vehicle constraints. The minimum turning radius is one of the most important ones. Besides the starting and ending points, the orientation of the angle is also crucial. Hence, if the curvature constraint is denoted as κ, the path planning equation may be written as:

$$P_i(x_i,\ y_i,\ \psi_i) \xrightarrow{\kappa} P_f(x_f,\ y_f,\ \psi_f) \qquad (2)$$

If an unmanned vehicle flyes around a circle at constante velocity, the circle radius and turning angular velocity can be described as follows:

$$R_{min} = \frac{v^2}{g\sqrt{n^2 - 1}} \tag{3}$$

To be able to obtain the smallest turning radius, the highest load factor and a low velocity are required. Likewise, to get an important turning rate, the largest possible load factor is also needed. The minimum velocity is selected. At any velocity the maximum load factor for a continuous turning flight is limited by the available thrust. [2,7,12].

$$\omega = \frac{g\sqrt{n^2 - 1}}{v} \tag{4}$$

In which n is the load factor and g is the gravity acceleration. The equations described previously are based on the aircraft dynamic performance. There is another possible way to calculate the minimum turning radius. It is shown in [11] as:

$$\rho_{min} = \frac{v^2}{g \ tan \ \phi_{max}} \tag{5}$$

The following expression is a manner to show the equations applied to compute start and finish circles based on the vehicle performance:

for $C_i(x_{ci}, \ y_{ci})$:

$$C_{x_{ci}} = x_i + R_{min} \ cos \ \left(\psi_i + \frac{\pi}{2}\right) \tag{6}$$

$$C_{y_{ci}} = y_i + R_{min} \ sin \ \left(\psi_i + \frac{\pi}{2}\right) \tag{7}$$

and for $C_f(x_{cf}, y_{cf})$:

$$C_{x_{cf}} = x_f + R_{min} \ cos \ \left(\psi_f + \frac{\pi}{2}\right) \tag{8}$$

$$C_{y_{cf}} = y_f + R_{min} \ sin \ \left(\psi_f + \frac{\pi}{2}\right) \tag{9}$$

Similarly, the angle ψ_L is the angle measured from the straight line segment $\chi_{(ci-cf)}$ to the y axis is given as follows:

$$\psi_L = \psi_{ci-cf} = tan^{-1} \left(\frac{y_{cf} - y_{ci}}{x_{cf} - x_{ci}}\right) \tag{10}$$

The shortest path is estimated by matching the distance between the center of the circles. The distance between the center of the circles CR_i and CR_f is calculated as:

$$\chi_{(ci-cf)} = \sqrt{(x_{cf} - x_{ci})^2 + (y_{cf} - y_{ci})^2}$$ (11)

The total length of the Dubins path is given by:

$$\chi_{Dubins} = \chi_{arci} + \chi_{tangent} + \chi_{arcf}$$ (12)

3.2 Dubins Airplane Paths

There is an option to get a 3D model. A significant analysis associated to disturbances is that wind is not considered in the equations of motion when the Dubins aircraft model is utilized. Thus, the kinematics model can be described as:

$$\begin{bmatrix} \dot{x} \\ \dot{y} \\ \dot{z} \\ \dot{\psi} \end{bmatrix} = \begin{bmatrix} v \ cos \ \gamma \ cos \ \psi \\ -v \ cos \ \gamma \ sin \ \psi \\ v \ sin \ \gamma \\ \omega \end{bmatrix}$$ (13)

where v is the airspeed, ψ is the heading angle and γ is the angle of flight. The relationship between the yaw angle ψ and the roll or bank angle ϕ is as follows:

$$\dot{\psi} = \frac{g}{v} \ tan \ \phi$$ (14)

where g is the gravity acceleration. Another hypothesis taken into consideration is that the well-tuned autopilot. So, the airframe model can be given as follows: [3,10,11].

$$\begin{pmatrix} \dot{x} = v \ cos \ \psi \ cos \ \gamma \\ \dot{y} = -v \ sin \ \psi \ cos \ \gamma \\ \dot{z} = v \ sin \ \gamma \\ \dot{\psi} = \frac{g}{v} \ tan \ \phi \end{pmatrix}$$ (15)

The height of the vehicle could be modified if the flight path angle γ is changed. Moreover, the physical aircraft restrictions set some limitations to both roll and flight path angles. Such restrictions are shown as: [14].

$$|\phi^c| = \leqslant \bar{\phi}$$ (16)
$$|\gamma^c| = \leqslant \bar{\theta}$$ (17)

Table 1. Dubins parameters for quadrotor paths

Dubins Path	R_{min}	γ_{max} (rad)	ψ_i	ψ_f	H_i	H_f	S_{Dubins}
RSR Low altitude	5 m	1.22	0.34	4.01	100	170	210.5 m
RSR High altitude	5 m	1.22	0.34	4.712	100	300	218.62 m
RSL Low altitude	5 m	1.22	5.75	−6.8	150	200	145.07* m
RSL High altitude	5 m	1.22	5.2	−6.8	350	450	147.85* m
LSR Low altitude	5 m	1.22	1.22	1.22	100	350	153.2 m
LSR High altitude	5 m	1.22	1.22	1.22	200	350	230.82 m
LSL Low altitude	5 m	1.22	1.22	−2.35	350	90	149.8 m
LSL High altitude	5 m	1.22	−1.22	−2.35	350	100	233.18 m

3.3 The Shortest Dubins Paths

In the RSR case, the total length is as follows:

$$
\begin{aligned}
\chi_{Dubins1} = {} & \varphi_i R_{min} \left[\left(\psi_L - \frac{\pi}{2} \right) - \left(\psi_i - \frac{\pi}{2} \right) \right] \\
& + \chi_{tangent(ci-cf)} + \varphi_f R_{min} \left[\left(\psi_f - \frac{\pi}{2} \right) - \left(\psi_L - \frac{\pi}{2} \right) \right]
\end{aligned}
\tag{18}
$$

where φ points how the path is moving along the arcs of the circles. The directions can be clockwise or counter-clockwise as shown in Fig. 1.

In the RSL case (Fig. 4), the total length is:

$$
\begin{aligned}
\chi_{Dubins2} = {} & \sqrt{\chi^2_{(c_i-c_f)} - 4R^2_{min}} + R_{min} \left[(\psi_L + \varphi_i + \psi_l) - \psi_L \left(\psi_i - \frac{\pi}{2} \right) \right] \\
& + R_{min} \left[(\psi_L + \pi) - \left(\psi_f + \frac{\pi}{2} \right) \right]
\end{aligned}
\tag{19}
$$

With respect to LSR path (Fig. 3), the total length is given by:

$$
\begin{aligned}
\chi_{Dubins3} = {} & \sqrt{\chi^2_{(c_i-c_f)} - 4R^2_{min}} + R_{min} \left[\left(\psi_i + \frac{\pi}{2} \right) - (\psi_L + \varphi_i \psi_l) \right] \\
& + R_{min} \left[\left(\psi_f - \frac{\pi}{2} \right) - (\psi_l + \psi_L + \varphi_i \psi_l - \pi) \right]
\end{aligned}
\tag{20}
$$

The LSL case looks similar to the RSR path (Fig. 2). Thus, the total length can be given as follows:

$$
\begin{aligned}
\chi_{Dubins4} = {} & \varphi_i R_{min} \left[\left(\psi_f + \frac{\pi}{2} \right) - \left(\psi_L + \frac{\pi}{2} \right) \right] \\
& + \chi_{(c_i-c_f)} + \varphi_f R_{min} \left[\left(\psi_L + \frac{\pi}{2} \right) - \left(\psi_f + \frac{\pi}{2} \right) \right]
\end{aligned}
\tag{21}
$$

Table 2. Flight angle computation

Flight Path Angle γ
RSR Low altitude $= 0.75\,\text{rad}$
RSR High altitude $= 0.73\,\text{rad}$
RSL Low altitude $= 0.33\,\text{rad}$
RSL High altitude $= 0.6\,\text{rad}$
LSR Low altitude $= 0.9\,\text{rad}$
LSR High altitude $= 0.57\,\text{rad}$
LSL Low altitude $= 0.78\,\text{rad}$
LSL High altitude $= 0.77\,\text{rad}$

Table 3. Roll angle computation

Roll angle ϕ
$\phi = 1.53\,\text{rad}$

Table 4. Pitch angle computation

Pitch Angle θ
RSR Low altitude $= 1.75\,\text{rad}$
RSR High altitude $= 1.73\,\text{rad}$
RSL Low altitude $= 1.33\,\text{rad}$
RSL High altitude $= 1.6\,\text{rad}$
LSR Low altitude $= 1.9\,\text{rad}$
LSR High altitude $= 1.57\,\text{rad}$
LSL Low altitude $= 1.78\,\text{rad}$
LSL High altitude $= 1.77\,\text{rad}$

Table 5. Yaw angle computation

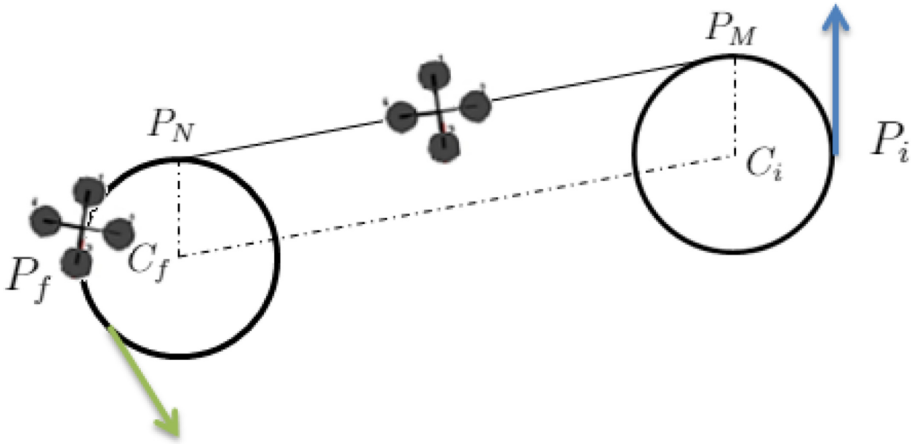| Yaw Angle ψ |
| --- |
| RSR Low altitude $= 1.52\,\text{rad}$ |
| RSR High altitude $= 1.54\,\text{rad}$ |
| RSL Low altitude $= 0.85\,\text{rad}$ |
| RSL High altitude $= 0.85\,\text{rad}$ |
| LSR Low altitude $= 0.84\,\text{rad}$ |
| LSR High altitude $= 0.84\,\text{rad}$ |
| LSL Low altitude $= 0.82\,\text{rad}$ |
| LSL High altitude $= 1.13\,\text{rad}$ |
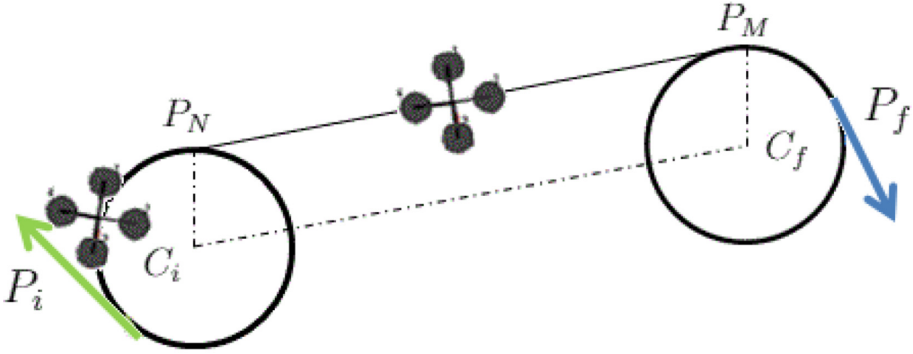
Fig. 1. RSR dubins path

Fig. 2. LSL dubins path

3.4   Helical Paths

A helical path can be described as follows:

$$p(t) = C_h + \begin{pmatrix} R_h \, \cos\,(\Pi_h \, t + \psi_h) \\ R_h \, \sin\,(\Pi_h \, t + \psi_h) \\ -t \, R_h \, \tan \theta_h \end{pmatrix} \tag{22}$$

Where $p(t) = [p_x \; p_y \; p_z]^T$ is the path position, and $C_h = [C_x \; C_y \; C_z]$ is the helix center. Hence, The initial helix position is given by:

$$p(0) = C_h + \begin{pmatrix} R_h \cos \psi_h \\ R_h \sin \psi_h \\ 0 \end{pmatrix} \tag{23}$$

Where R_h is the radius, $\Pi = +1$ denotes that the helix rotates in a clockwise direction and $\Pi = -1$ is the opposite direction. θ_h is the helix path angle.
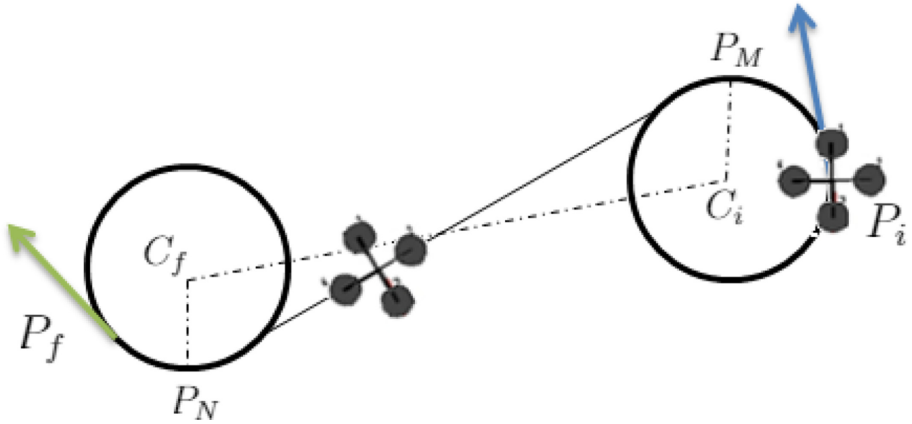
Fig. 3. LSR dubins path
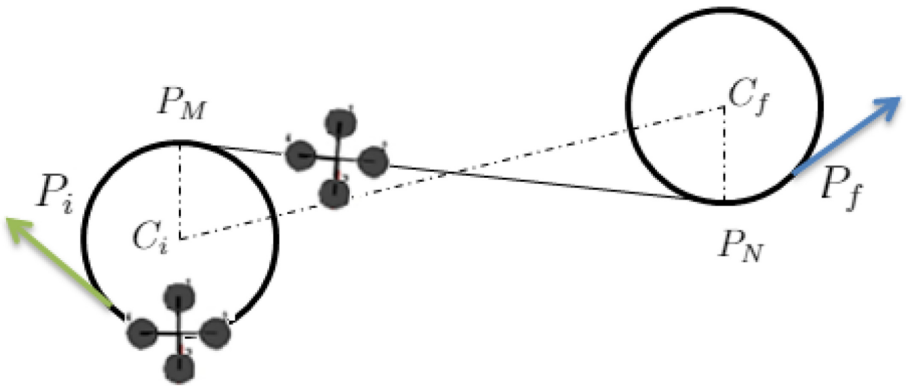
Fig. 4. RSL dubins path

Therefore, a helical path can be expressed as:

$$\mathcal{P}_h = (C_h \ \psi_h \ \Pi_h \ R_h \ \theta_h) \tag{24}$$

Several values for θ_{max}, ψ_{max}, ψ_{min}, H_i, H_f and R_{min} are given (Table 1). Possible Dubins paths for a quadrotor are generated and presented in the following figures. These types of paths applicable when a a quadrotor is flying at a steady speed and when roll and pitch angles have certain constraints. The velocity considered is about 15 m/s. The minimum radius is decreased to avoid large arcs and keep VTOL features. This particular detail show the way to compute a maximum flight path angle γ of 1.22 radians. It is a close constraint value as in [14]. In addition, Eq. 10 is used to find the flight path angle values (Tables 2, 3, 4). In the same way, pitch and roll angles (ϕ θ, ψ) are computed by applying the equations that follow:
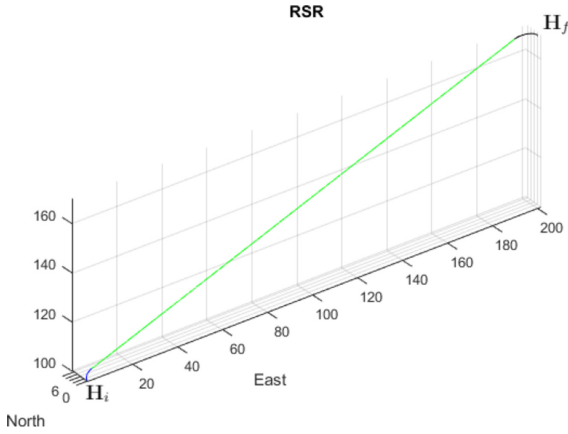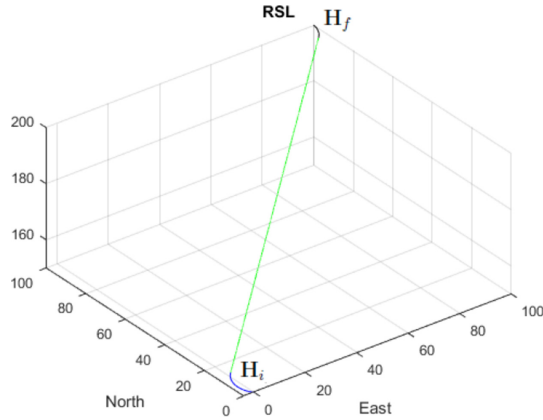
Fig. 5. RSR dubins path low altitude
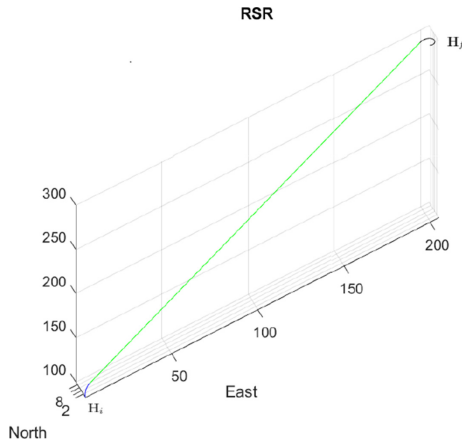

Fig. 6. RSR dubins path high altitude

$$\theta = \alpha_a + \gamma$$
$$\phi = tan^{-1} \frac{v^2}{R_{min}} \tag{25}$$

and the heading angle is found by using Eq. 30. These calculations are done just for the Dubins paths that are a suitable choice for a quadrotor with a + configuration. Dubins airplane paths are more complicated because of the altitude variable included. The path cases are determined by the difference of the altitude between the start and final positions. These are described as low, medium and high altitude [6,14]. H is be taken as z for altitude regarding to start and final configurations or altitude difference. Low and high alternatives are only taken in this research work. The path climbs and descends from H_i to

Fig. 7. RSL dubins path for low altitude
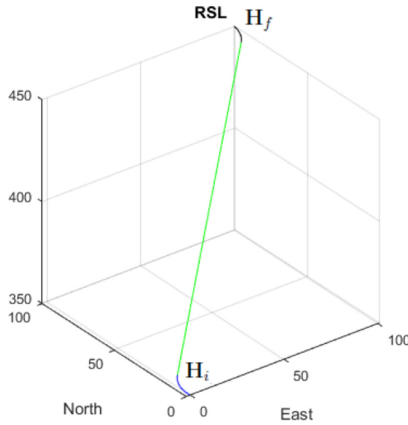
Fig. 8. RSL dubins for high altitude

H_f when γ is varied. So, it can be as follows (Table 5):

$$\gamma = tan^{-1} \left(\frac{H_f - H_i}{\chi_{tangent}} \right) \tag{26}$$

4 Results

As it is given in Table 1, different values for θ_{max}, ψ_{max}, ψ_{min}, H_i, H_f and R_{min} are determined. (R_{min}, γ_{max} and ϕ are constant). A low level autopilot is included into the computational resource with common aeronautics symbols. It changes within commands of straight lines and helical paths. Also orientation regulation is also adjusted. All Dubins paths are performed for both altitude cases (low and high). A helix parameter is considered as well. However, it is
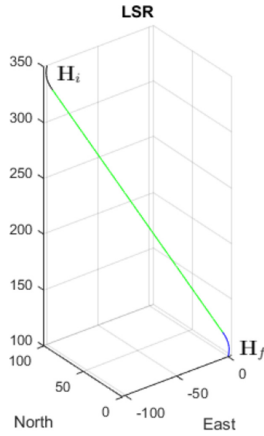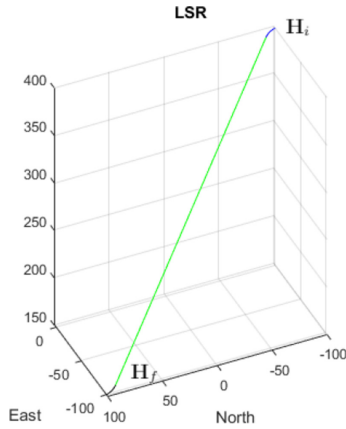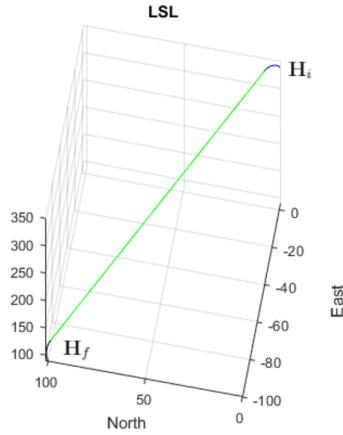
Fig. 9. LSR dubins path low altitude

Fig. 10. LSR dubins path high altitude

not really accomplished because of the set values and path conditions. It can suggested that the RSL is the shortest path. Quadrotor attitude parameters are established. Thus, after calculating flight angles, all of seem very small without significant variations. Also, the pitch and yaw angles are also very similar specially, the RSL ones at low altitudes. The generated paths are shown in the following graphs (Figs. 5, 6, 7, 8, 9, 10, 11 and 12).

Fig. 11. LSL dubins path low altitude
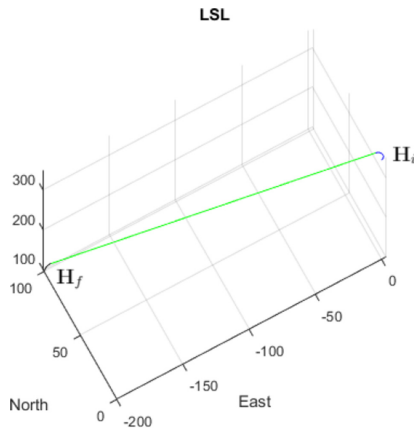
Fig. 12. LSL dubins path high altitude

5   Conclusions

It can be inferred that a quadrotor can truly fly in RSR, RSL, LSL and LSR path types keeping a constant minimum radius and velocity. This method has been implemented as an useful way to measure the shortest path with the maximum curvature for an unmanned aerial airplane based on different estimated points. Additionally, a modification of the Dubins car model is established. Thus, another way for turning flight might be achieved just by taking a constant velocity. Therefore, very similar paths with no Dubins curves can be performed. It is observed that helical paths are not easily got or are not really necessary to get the initial and final points. This factor is because of the VTOL characteristics of this type of airplane. Likewise, it appears to be that the integrated autopilot

needs proper adjustments. Attitude angles can be computed from basics flight dynamics equations.

References

1. Alexis, K Dr.: Dubins Airplane. http://www.kostasalexis.com/dubins-airplane.html. (2017)
2. Anderson, J.D.: Aircraft performance and design. McGraw-Hill international editions: Aerospace science/technology series. WCB/McGraw-Hill, New York (1999). ISBN: 9780070019713. https://books.google.com.co/books?id=PwtO7aiwbBwC
3. Cárdenas, C.A., Grisales, V.H., Collazos Morales, C.A., Cerón-Muñoz, H.D., Ariza-Colpas, P., Caputo-Llanos, R.: Quadrotor Modeling and a PID Control Approach. In: Tiwary, U.S., Chaudhury, S. (eds.) IHCI 2019. LNCS, vol. 11886, pp. 281–291. Springer, Cham (2020). https://doi.org/10.1007/978-3-030-44689-5_25
4. Beard, R.W., McLain, T.W.: Small Unmanned Aircraft: Theory and Practice. Princeton University Press, New Jersey (2012)
5. Cárdenas Ruiz, C.A.: Performance study of the flight control and path planning for a UAV type Quadrotor. In: Ingeniería Mecatrónica (2018)
6. Chitsaz, H., LaValle, S.M.: Time-optimal paths for a Dubins airplane. In: Decision and Control, 2007 46th IEEE Conference on, pp. 2379–2384. IEEE (2007)
7. Collazos, C., et al.: State estimation of a dehydration process by interval analysis. In: Figueroa-García, J.C., López-Santana, E.R., Rodriguez-Molano, J.I. (eds.) WEA 2018. CCIS, vol. 915, pp. 66–77. Springer, Cham (2018). https://doi.org/10.1007/978-3-030-00350-0_6
8. Dubins, L.E.: On curves of minimal length with a constraint on average curvature, and with prescribed initial and terminal positions and tangents. Am. J. Math. **79**(3), 497–516 (1957)
9. Grymin, D.: Development of a novel method for autonomous navigation and landing of unmanned aerial vehicles. In: (2009)
10. Li, W., et al.: A 3D path planning approach for quadrotor UAV navigation. In: Information and Automation, 2015 IEEE International Conference on, pp. 2481–2486. IEEE (2015)
11. Lugo-Cárdenas, I., et al.: Dubins path generation for a fixed wing UAV. In: Unmanned Aircraft Systems (ICUAS), 2014 International Conference on, pp. 339–346. IEEE (2014)
12. Cárdenas, R.C.A., et al.: Mathematical Modelling and Identification of a Quadrotor. In: Gervasi, O., et al. (eds.) ICCSA 2020. LNCS, vol. 12249, pp. 261–275. Springer, Cham (2020). https://doi.org/10.1007/978-3-030-58799-4_19
13. Omar, R.B.: Path planning for unmanned aerial vehicles using visibility line-based methods. PhD thesis. University of Leicester (2012)
14. Owen, M., Beard, R.W., McLain, T.W.: implementing Dubins airplane paths on fixed-wing UAVs*. In: Valavanis, K.P., Vachtsevanos, G.J. (eds.) Handbook of Unmanned Aerial Vehicles, pp. 1677–1701. Springer, Dordrecht (2015). https://doi.org/10.1007/978-90-481-9707-1_120
15. Pharpatara, P.: Trajectory planning for aerial vehicles with constraints. Theses. Université Paris-Saclay; Université d'Evry-Val-d'Essonne, September (2015). https://tel.archives-ouvertes.fr/tel-01206423
16. Poyi, G.T.: A novel approach to the control of quad-rotor helicopters using fuzzy-neural networks. In: (2014)

17. Shanmugavel, M., et al.: Path planning of multiple autonomous vehicles. In: (2007)
18. Antonios Tsourdos, Brian White, and Madhavan Shanmugavel. Cooperative Path Planning of Unmanned Aerial Vehicles. vol. 32. Wiley, Chichester (2010)
19. Valavanis, K.P., Vachtsevanos, G.J. (eds.): Handbook of Unmanned Aerial Vehicles. Springer, Dordrecht (2015). https://doi.org/10.1007/978-90-481-9707-1